nature biotechnology

Control of phosphorothioate stereochemistry substantially increases the efficacy of antisense oligonucleotides

Naoki Iwamoto[1,4], David C D Butler[1,4], Nenad Svrzikapa[1,4], Susovan Mohapatra[1], Ivan Zlatev[1,3], Dinah W Y Sah[1,3], Meena[1], Stephany M Standley[1], Genliang Lu[1], Luciano H Apponi[1], Maria Frank-Kamenetsky[1], Jason Jingxin Zhang[1], Chandra Vargeese[1] & Gregory L Verdine[1,2]

Whereas stereochemical purity in drugs has become the standard for small molecules, stereoisomeric mixtures containing as many as a half million components persist in antisense oligonucleotide (ASO) therapeutics because it has been feasible neither to separate the individual stereoisomers, nor to synthesize stereochemically pure ASOs. Here we report the development of a scalable synthetic process that yields therapeutic ASOs having high stereochemical and chemical purity. Using this method, we synthesized rationally designed stereopure components of mipomersen, a drug comprising 524,288 stereoisomers. We demonstrate that phosphorothioate (PS) stereochemistry substantially affects the pharmacologic properties of ASOs. We report that *S*p-configured PS linkages are stabilized relative to *R*p, providing stereochemical protection from pharmacologic inactivation of the drug. Further, we elucidated a triplet stereochemical code in the stereopure ASOs, 3′-*S*p*S*p*R*p, that promotes target RNA cleavage by RNase H1 *in vitro* and provides a more durable response in mice than stereorandom ASOs.

ASO therapeutics are DNA analogs that hybridize to their mRNA targets in a sequence-specific manner. ASOs can impede protein expression via several mechanisms, one of which involves the formation of an ASO–mRNA heteroduplex that triggers RNase H1 activity, mRNA degradation, and consequently, downregulation of protein expression[1,2]. Decades of research have yielded numerous chemical modifications that have improved the activity of ASO drugs, and there are now many in development[3,4]. The PS group is among the most ubiquitous and important of these modifications, improving the metabolic stability and cellular uptake of ASOs without substantially compromising their affinity for target mRNA or RNase H1 activity[5].

PS substitution converts the achiral phosphodiester (PO) linkage into a chiral PS center having two distinct stereochemical configurations, designated *S*p and *R*p (**Fig. 1a**). Because there has existed no practical means to control the geometry of PS installation, all PS-substituted ASOs comprise mixtures of up to 2^n individual drug molecules, where n equals the number of PS linkages. For example, mipomersen, approved by the US Food and Drug Administration (FDA) to treat homozygous familial hypercholesterolemia, contains 19 PS linkages and hence consists of over half a million individual stereoisomers[6]. Dozens of such ASO mixtures are presently in clinical development. It is well-established that stereochemical variation at even a single stereogenic center in small molecules can profoundly affect their pharmacologic properties, (http://www.fda.gov/Drugs/GuidanceComplianceRegulatoryInformation/Guidances/ucm122883.htm). Hence it seemed possible that stereoisomeric ASOs might exhibit distinct behaviors *in vitro* and *in vivo*.

Several groups have previously reported the chemical synthesis of oligonucleotides with defined stereochemistry of PS linkages, but none has proved sufficiently robust and generalizable for the stereoprogrammable synthesis of therapeutically relevant ASOs. The pioneering work of Stec *et al.* on oxathiaphospholanes[7,8] enabled the chemical synthesis of stereopure PS-substituted oligonucleotides, but the poor coupling efficiency of this method limits its scope to basic research applications. The oxazaphospholidine approach[9,10] improved coupling efficiency but suffers from poor stereochemical selectivity in the coupling reaction. The *N*-acyl oxazaphospholidine method[11] is effective in providing only short sequences (12 mers) and in limited yield.

A method that combines high stereochemical selectivity and high coupling efficiency, even with 2′-modified substrates, is the oxazaphospholidine approach[12–14]. Even this method, however, suffers from the challenges associated with post-synthetic removal of the chiral auxiliary, which precluded in practical terms the synthesis of any sequence longer than 12 oligomers[15]. An H-phosphonate-based approach solved the problem of auxiliary removal but is incompatible with capping of truncated sequences, thereby making purification impractical[16]. Thus, despite these and other attempts, no practical and scalable method for the synthesis of stereopure PS oligonucleotides, other than all-*S*p or all-*R*p, having pharmaceutical-grade purity has been reported.

We developed a method for stereocontrolled synthesis of PS ASOs that uses nucleoside 3′-oxazaphospholidine derivatives as monomers

[1]Wave Life Sciences, Cambridge, Massachusetts, USA. [2]Department of Stem Cell and Regenerative Biology, Department of Chemistry and Chemical Biology, Harvard University and Harvard Medical School, Cambridge, Massachusetts, USA. [3]Present addresses: Alnylam Pharmaceuticals, Cambridge, Massachusetts, USA (I.Z.). and Voyager Therapeutics, Cambridge, Massachusetts, USA (D.W.Y.S.). [4]These authors contributed equally to this work. Correspondence should be addressed to G.L.V. (gregory_verdine@harvard.edu).

Received 22 September 2016; accepted 26 July 2017; published online 21 August 2017; doi:10.1038/nbt.3948

but employs a distinct synthesis procedure termed SOSICS (stereocontrolled oligonucleotide synthesis with iterative capping and sulfurization), with a sequence of capping and sulfurization leading to efficient, spontaneous release of the chiral auxiliary (**Fig. 1b**; **Supplementary Note**, **Supplementary Figs. 1** and **2** and **Supplementary Tables 1** and **2**). We applied the SOSICS method to test whether backbone stereochemistry affects the pharmacologic properties of PS ASOs, using mipomersen as a benchmark. Mipomersen is a gapmer ASO containing five 2′-*O*-methoxyethyl (MOE)-modified nucleotides at each end of the molecule that are less toxic, have higher affinity for the target RNA and are resistant to exonucleases compared with unmodified nucleotides[6]. Mipomersen targets *APOB100* mRNA, which encodes the main structural protein of low-density lipoprotein cholesterol, and is FDA-approved for the treatment of homozygous familial hypercholesterolemia. We evaluated the pharmacological differences between mipomersen as a complex diastereomeric mixture and mipomersen that was rationally designed of chirally pure components. We show that stereochemistry affects important pharmacological properties of mipomersen components. Based in part on analysis of the X-ray crystal structure of human RNase H1 in complex with a RNA–DNA heteroduplex, we discovered a backbone stereochemical code that increases the efficiency of mRNA cleavage *in vitro* and the durability of its impact *in vivo*.

RESULTS

A stereo-controlled synthetic platform

The first step of the SOSICS cycle entails coupling of a stereochemically pure nucleoside oxaphospholidine monomer (**Fig. 1b**, *Sp*1 or *Rp*1, Step 1) to the 5′-oxygen of a resin-bound nucleoside or oligonucleotide, a reaction that proceeds with high chemical conversion and clean inversion of stereochemical configuration[16]. The resulting trialkyl-phosphite-containing species is subjected to standard capping with phenoxyacetic anhydride (Step 2), which caps truncated sequences and facilitates subsequent auxiliary removal via acylation of the pyrrolidine nitrogen on the chiral auxiliary. The nucleophilic phosphorus atom of the trialkyl phosphite is then subjected to attack by an electrophilic sulfurizing reagent, *S*-cyanoethyl methylthiosulfonate[17], whereupon the chiral auxiliary is released[18], leading to an *S*-cyanoethyl phosphorothioate triester having complete retention of stereochemical configuration with respect to the attacking lone pair on phosphorus (Step 3). Next, the 5′-dimethoxytrityl protecting group is removed to expose a new 5′-hydroxy terminus suitable for coupling in the next cycle (Step 4).

Steps 1–4 are performed iteratively until the oligonucleotide chain has been fully elaborated, at which time the *S*-cyanoethyl protecting groups are removed by conjugate elimination on the synthesis resin, and finally the oligonucleotide is released from the resin and all the nucleobase-protecting groups are removed in one reaction step. In the SOSICS synthesis method, the stereochemistry of each PS linkage is individually programmed by selection of the appropriate chiral building block in Step 1. Following routine purification, this method provides oligonucleotide products having both high chemical and stereochemical purity, in yields sufficient for studies in animal models (**Supplementary Note**, **Supplementary Fig. 2** and **Supplementary Table 1**).

Design and synthesis of stereochemically pure components of mipomersen

We applied the SOSICS approach to generate a panel of stereochemically pure oligonucleotide components of mipomersen (**Fig. 1c**) to test the impact of stereochemistry on pharmacological parameters. Because it is impractical to synthesize and test all 524,288 components

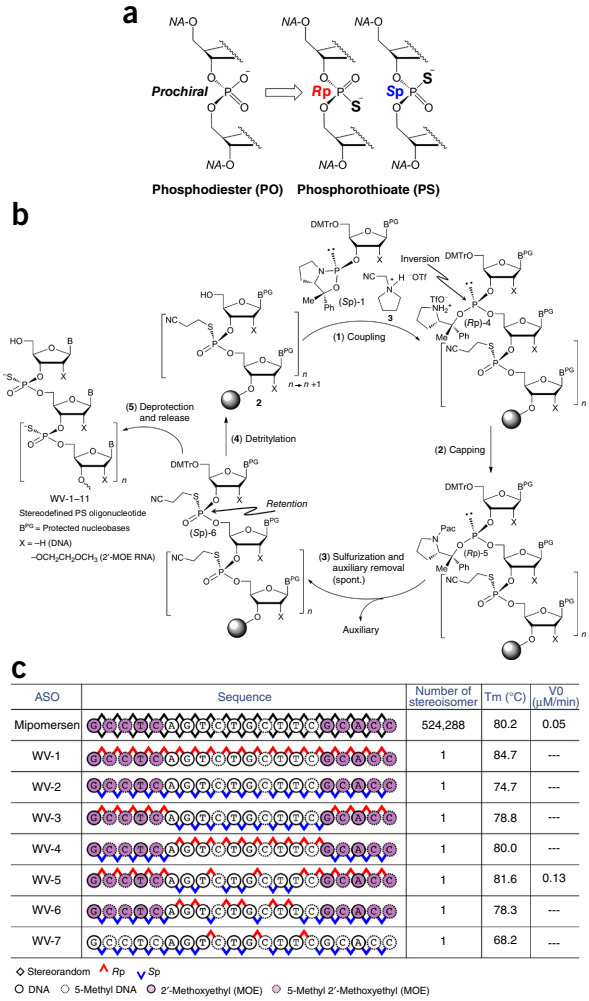

Figure 1 The synthesis cycle of the SOSICS method. (**a**) Structure of phosphodiester (PO) and phosphorothioate (PS) linkages illustrating the introduction of chirality with the sulfur and the resulting *Sp* (blue) and *Rp* (red) linkages. (**b**) The SOSICS cycle is composed of five major steps: (1) Coupling: 0.15 M chiral phosphoramidite **1** with 2.0 M *N*-(cyanomethyl)pyrrolidinium trifluoromethanesulfonate (CMPT) **3** was coupled to 5′-OH oligonucleotide attached to the support **2** to give phosphite intermediate **4**. (2) Capping: **4** was treated with 5wt% phenoxyacetic anhydride in tetrahydrofuran to acetylate the amine on chiral auxiliary and 5′-OH of failure sequences. (3) Sulfurization: **5** was treated with 0.3 M CNE-MTS (*S*-cyanoethyl-methylthiosulfonate) and 0.1 M *N,O*-bistrifluoroacetamide (BSTFA) in acetonitrile to give *S*-cyanoethyl phosphorothioate **6** with the removal of chiral auxiliary. (4) Detritylation: 5′-DMTr (4,4′-dimethoxytrityl) group of **6** was removed by 3wt% trichloroacetic acid (TCA) in dichloromethane. (5) Deprotection and release: cyanoethyl groups of **6** were removed by 0.5 M 1,5-diazabicyclo(4.3.0)non-5-ene (DBN), 0.25 M BSTFA in acetonitrile, and oligonucleotide was released and protecting groups on nucleobases were removed with 28% aqueous ammonia to give WV-**1**-**6**. B^{PG} Protected nucleobase, X: -H (DNA), $-OCH_2CH_2OCH_3$ (2′-MOE RNA). (**c**) Mipomersen and its stereochemically pure counterparts. All ASOs are 20-mer PS oligonucleotides composed of 10-nucleotide DNA cores and 2′-MOE-modified ends. C is 5MeC in all instances. Complementary RNA strand (human *APOB100* mRNA): rGrGrUrGrCrGrArArGrCrArGrArCrUrGrArGrGrC. WV-1 and WV-2 have uniform stereochemistry, all-Rp and all-Sp, respectively. WV-3 and WV-4 have inverse patterns of stereochemistry, which are uniform within each gapmer component (the core and ends), but differ between the two (Rp5-Sp10-Rp4 and Sp5-Rp10-Sp4, respectively). WV-5 has all-*Rp* ends and an $(RpSpSp)_3$ core (denoted SSR); WV-6 has all-*Sp* ends and an $(SpRpRp)_3$ core (denoted *RRS*). Tm was calculated by annealing the ASOs to a synthetic oligo comparable to human *APOB100* mRNA.

of mipomersen, we applied rational design principles to generate a small panel of molecules to explore the most relevant stereochemical permutations. We applied conventional phosphoramidite chemistry to generate mipomersen for comparison[6].

We designed WV-1 and WV-2 to test the impact of stereochemically uniform PS substitutions with all-*Rp* and all-*Sp* configurations, respectively. WV-3 and WV-4 test the effect of stereochemically uniform substitution in gapmer components, the 2′-MOE ends and the 10-nucleotide DNA core. WV-5 and WV-6 were rationally designed based on the stereochemistry of protein contacts to the prochiral non-bridging phosphate oxygen atoms observed in the X-ray structure of RNase H1 bound to an RNA–DNA heretoduplex. When the catalytic domain of RNase H1 binds to an RNA–DNA heteroduplex, it directly contacts three contiguous PO linkages on the DNA strand (**Fig. 2a**) and cleaves the RNA at a scissile phosphate located two nucleotides further downstream with respect to the RNA[19]. At each of the three PO linkages, amino acids of RNase H1 contact the prochiral non-bridging phosphate oxygens in a stereochemically differentiated manner (**Fig. 2b**). For example, at the 3′-end of the trinucleotide, the indole ring of Trp225 contacts only the pro-*S* oxygen, and the amide backbone of Ser223 contacts only the pro-*R* oxygen. Such stereochemically differentiated contacts are typically energetically inequivalent, so they should respond differently to functional group substitution of O by S. Hence, it seemed possible that RNase H1 might be sensitive to PS stereochemistry at its three contacted backbone phosphates, and we further reasoned that the 3′-*SpSpRp*-5′ (using antisense-strand directionality, hereafter denoted as *SSR*) might be preferred. In WV-5, we maintained the same all-*Rp* configuration in the 2′-MOE wings as WV-3, but we changed the central segment from all-*Sp* to three tandem repeats of *SSR*. WV-6 bears the same wings as WV-4 (all-*Sp*) but with a central segment containing three tandem repeats of *RRS*.

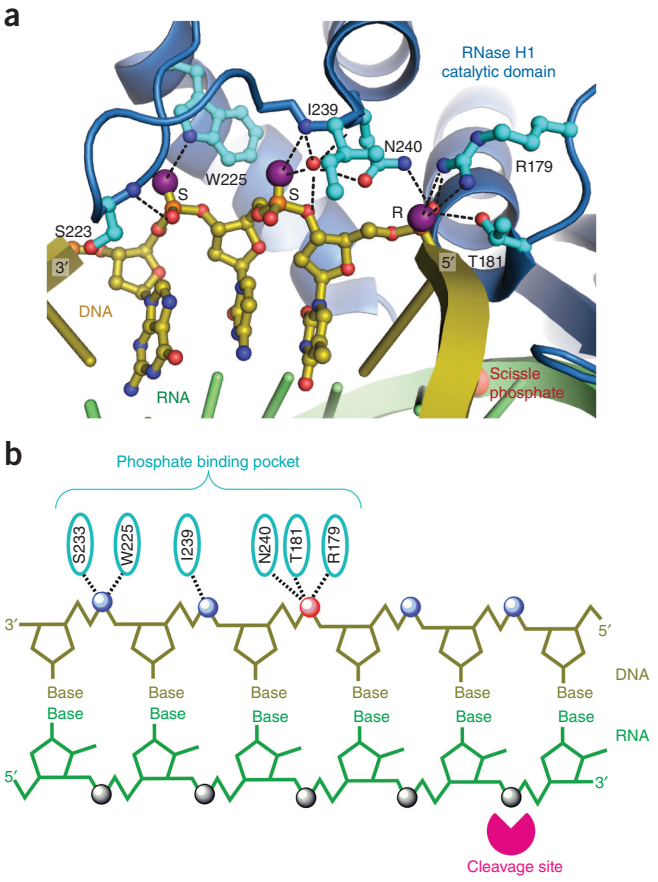

Figure 2 The stereochemical preferences of RNase H1. (**a**) A 3D view of the RNase H binding and catalytic sites in complex with an RNA–DNA heteroduplex[19]. (**b**) A 2D view of an RNA–ASO heteroduplex showing contacts and cleavage sites of RNase H1. The ASO (top) contains PS linkages with the SSR code (S blue; R red). The target mRNA (bottom) is cleaved downstream of the RNase H1 binding site (illustrated by the brackets); the cleavage location is denoted. Amino acids in RNase H1 that directly contact the phosphates of ASO are shown (phosphate-binding pocket).

Thermal stability

Because RNA–DNA heteroduplex formation is necessary for RNase H activity, the thermal stability of ASO–RNA duplexes affects the activity of the ASO. To determine the extent to which stereochemistry affects thermal stability, we measured the melting temperature (Tm) of heteroduplexes containing mipomersen or several of its components (**Fig. 1c**). The Tm of WV-2 (all-*S*) was 74.7 °C, whereas the Tm of WV-1 (all-*R*) was 84.7 °C, indicating that *Rp* PS modifications increase thermal stability compared with *Sp* linkages, which is consistent with prior reports[20]. Tm data for the remaining components follow this same general trend (WV-1 > WV-5 > WV-4 > WV-3 > WV-6 > WV-2 for stability and number of *Rp* linkages). PS stereochemistry thus affects thermal stability, though only to the modest extent of ~0.5 °C per PS linkage (*Rp* > *Sp*), which in most cases would be insufficient to justify favoring one PS stereochemistry over the other.

Sp linkages increase lipophilicity

Lipophilicity broadly affects the pharmacologic properties of drugs, especially tissue penetration and *in vivo* half-life, because of its effect on serum-protein binding. Though all-*Rp* and all-*Sp* PS ASOs are known to exhibit different lipophilicities[21], the impact of position-specific stereochemical variations on lipophilicity has not been tested. We evaluated the lipophilicity of our panel of ASOs by assessing retention times on a C18 reversed-phase high-performance liquid chromatography (HPLC) column. Consistent with mipomersen being a complex stereochemical mixture of inseparable components, the drug eluted as a broad, featureless and symmetrical peak (**Fig. 3a**, upper panel). By contrast, the stereopure components all exhibited sharp peaks, with a wide range of elution times (**Fig. 3a**, lower panel), indicating that PS stereochemistry has a marked impact on the overall lipophilicity of the molecule. It is worth noting that the all-*Rp* (WV-1) and all-*Sp* (WV-2) components both lie outside the main elution envelope of mipomersen, though they are present in such minor amounts in mipomersen that neither exhibited a clear peak. When we examined the ionic character of the PS oligonucleotides by ion-exchange chromatography, we observed similar results; PS stereochemistry markedly alters the ionic character of the molecules, and mipomersen exhibits wide-ranging ionic behavior (**Supplementary Fig. 3** and **Supplementary Table 3**). Thus, PS stereochemistry can be exploited to tune the lipophilicity and ionic character of oligonucleotides.

Sp linkages increase the metabolic stability of ASOs *in vitro*

Nucleolytic degradation is the primary pathway leading to metabolic inactivation of oligonucleotides, and PS substitution decreases this degradation rate[5]. However, heretofore it has not been possible to assess systematically the impact of PS stereochemistry on nucleolytic degradation in ASOs having combinations of *Sp* and *Rp* PS linkages. To gain insight into this issue, we measured the nucleolytic stability of our stereo-defined ASOs. In rat whole liver homogenates, the stability of WV-1-6 varied dramatically as a function of PS stereochemistry

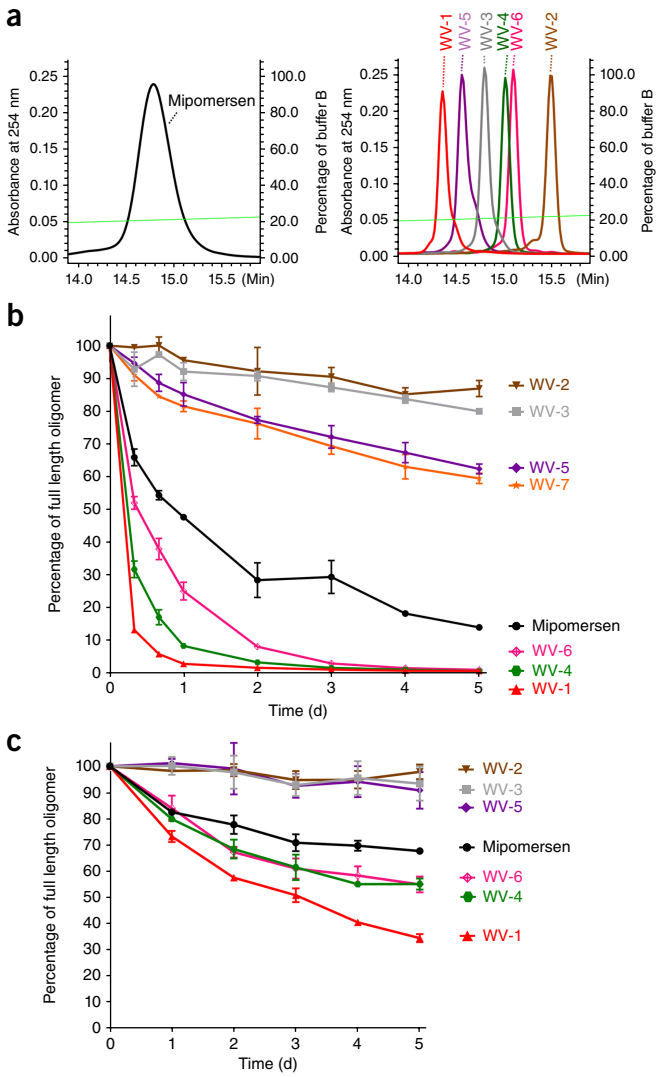

Figure 3 Stereochemistry affects ASO pharmacological properties *in vitro*. (**a**) Reversed-phase (RP) HPLC traces of mipomersen and rationally designed, chirally pure mipomersen components showing elution time (*x* axis) and absorbance at 254 nm (*y* axis). Light green curves show the gradient percentage buffer B. (**b**) Time-dependent stability of mipomersen and its stereopure components in rat liver homogenate, showing that *Sp* linkages promote ASO stability and *Sp* linkages can replace 2′-MOE modifications to stabilize ASOs. (**c**) Time-dependent stability of mipomersen and its stereopure components in rat serum, showing that *Sp* linkages in the gapmer core increase ASO stability.

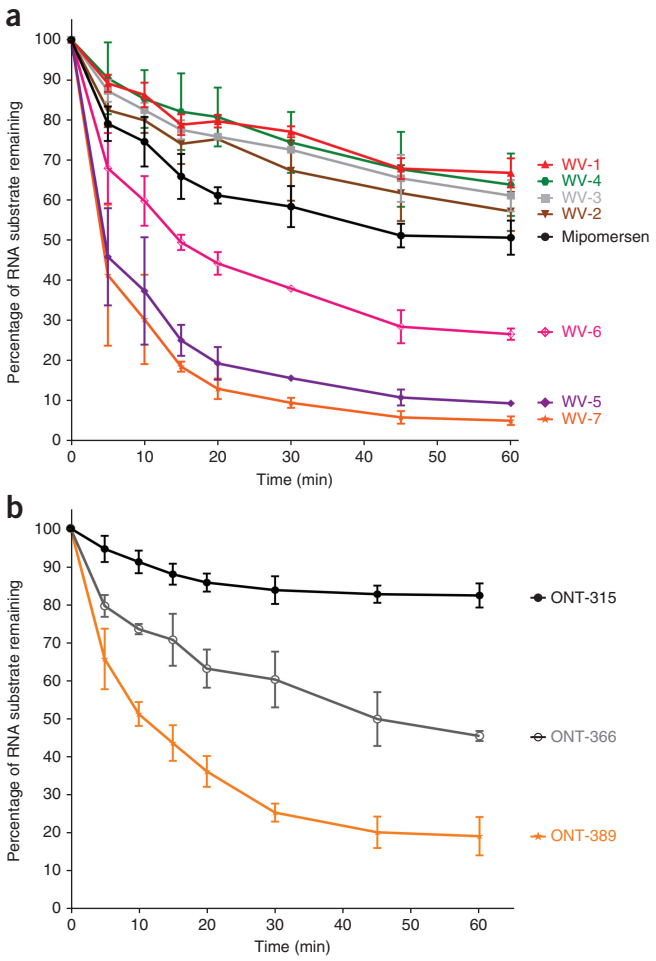

Figure 4 An *SSR* code promotes RNase HC activity *in vitro*. (**a**) Time-dependent activity of RNase HC *in vitro* on ASO–RNA heteroduplexes, showing stereochemistry in the gapmer core affects activity, with an *SSR* in the core providing maximal activity, and that *Sp* linkages can replace 2′-MOE modifications in the gapmer ends to promote activity. Both stereopure components (WV-5 and WV-7) were significantly more active than mipomersen ($P \leq 0.0001$, 2-way ANOVA). (**b**) The *SSR* code promotes RNase HC activity *in vitro*, independent of sequence. Time-dependent activity of RNase HC *in vitro* on ASO–RNA heteroduplexes, showing *SSR* stereochemistry code in the core provides maximal activity for ASOs targeting human *FOXO1* mRNA (see **Supplementary Fig. 3** for sequence and chemistry of ASOs).

(**Fig. 3b**). WV-1 (all-*Rp*) was completely degraded within 2 d, while WV-2 (all-*Sp*) showed negligible degradation even after 5 d. As expected, mipomersen's stability was comparable to the approximate average of the stereochemically pure all-*Rp* (WV-1) and all-*Sp* (WV-2) components. The remaining components fell between WV-1 and WV-2, with increasing *Rp* content in the DNA core correlating with faster degradation. Interestingly, WV-7, a component of mipomersen identical to WV-5 in the stereochemistry of the DNA core but with *Sp* linkages replacing the 2′-MOE-modified nucleotides at the ends, was as stable as WV-5 in rat liver homogenates for over 5 d, indicating that *Sp* linkages can stabilize ASOs to an extent comparable to the 2′-MOE modification. Thus, PS stereochemistry influences the metabolic stability of ASOs in rat liver homogenates, and increasing the proportion of *Sp* linkages increases their stability.

We also tested whether PS stereochemistry affects ASO stability *in vitro* in rat serum[22]. Similar to the rat liver homogenate results, the stability of WV-1 through WV-6 varied as a function of stereochemistry and followed the same general pattern from above, with WV-1 (all-*Rp*) being the least stable, WV-2 (all-*Sp*) being the most stable, and mipomersen falling in the middle (**Fig. 3c**). Overall these data indicate that *Sp* linkages, especially in the DNA core, increase ASO stability in rat serum.

An *SSR* code promotes RNase H1 activity

RNase H1 helps mediate the mechanism of action of ASOs. The 2′-MOE gapmer design increases an ASO's affinity for its mRNA target while maintaining RNase H1 sensitivity in the DNA core. 2′-MOE

modifications, however, decrease the number of available RNase H1 cleavage sites and the RNA cleavage rate[23]. Thus, it is important to understand how stereochemistry in the gapmer ASO affects the RNase H1 cleavage rate of the mRNAs target.

We measured the relative rates of cleavage by the human RNase H1 catalytic domain (RNase HC) as well as the initial velocity when the ASOs were duplexed with complementary RNA *in vitro*. The ASO-RNA heteroduplexes were differentially susceptible to cleavage (**Fig. 4a**). Mipomersen, WV-1, WV-2, WV-3 and WV-4 duplexes were weak substrates for RNase HC. WV-5 and WV-6 increased RNase HC cleavage rates, with WV-5, containing the *SSR* chirality motif, having the highest cleavage activity (V_0: mipomersen = 2.37 ± 0.20 μM/min; WV-5 = 6.90 ± 0.54 μM/min, **Supplementary Fig. 4**). Because all of the ASOs in this panel have 2′-MOE-modified wings, the differences in cleavage activity that we detect are attributable to the varying stereochemistry in the DNA core of each compound.

Both the rate and extent of RNase H1-dependent cleavage of the target RNA influence the efficacy of ASOs. Although previous reports have suggested that the RNase H1 cleavage rate of RNA–PS DNA duplexes is faster for all-*Rp* than all-*Sp* stereoisomers[24,25], our results demonstrate that RNase H1 is sensitive to the stereochemistry of the PS backbone. In general terms, we observed that increasing *Sp* content is associated with both an increased rate and a greater overall extent of target RNA cleavage. We also discovered that an *SSR* code provided more rapid and complete RNA cleavage than that observed with stereorandom ASOs.

To test whether *Sp* linkages, which stabilize ASOs, can replace 2′-MOEs on the ends and preserve the impact of the *SSR* motif on RNase HC activity, we generated WV-7, which has *Sp* linkages in place of 2′-MOEs in the gapmer ends but is identical to WV-5 in the core. WV-7 was comparable to WV-5 in promoting RNase H1 cleavage (**Fig. 4a**), and both stereopure components (WV-5 and WV-7) were significantly more active than mipomersen ($P \leq 0.0001$, $n = 3$, 2-way ANOVA). Thus, we concluded that *Sp* linkages in the gapmer ends can replace 2′-MOE-modified nucleotides for promoting stability *in vitro*, and combining *Sp* linkages in the ends with the *SSR* motif in the core can be comparable to the 2′-MOE plus *SSR* combination.

To ensure the *SSR* code is not specific to mipomersen, we tested the code using an ASO with unrelated sequence (ONT-389, **Supplementary Table 4**). We measured the relative rates of cleavage by RNase HC when each ASO, stereorandom or stereopure, was duplexed with its complementary human mRNA sequence. Similar to mipomersen, the stereorandom mixtures ONT-315 and ONT-366 were weak substrates for RNase HC, whereas the stereopure component ONT-389, with gapmer ends stabilized by *Sp* linkages and the *SSR* code, promoted RNase HC activity (**Fig. 4b**).

Stereochemistry affects *in vivo* potency and durability of responses

To determine whether PS stereochemistry affects ASO activity in biological systems, we first assessed that activity of mipomersen and its stereopure counterparts in cells via transfection (**Supplementary Fig. 5**). There is no correlation between the in-cell IC_{50}s and the activity of these ASOs. Because it is well-established in the ASO field that data obtained with ASOs transfected into cells in culture are not meaningfully predictive of *in vivo* activity[26], we proceeded to test the ASOs in animal models. To determine whether the effects of PS stereochemistry observed *in vitro* are also manifest *in vivo*, we assessed the activity of mipomersen and its stereochemically pure components in transgenic mice expressing human *APOB100* (ref. 27). We administered eight intraperitoneal doses of mipomersen or stereochemically pure components twice weekly for 4 weeks and assessed RNase H1 activity by measuring serum levels of human APOB100 protein and liver levels of *APOB100* mRNA (**Fig. 5a**,**b** and **Supplementary Figs. 6** and **7**). Notably, mipomersen, WV-5 and WV-6 led to a ~70% decrease in

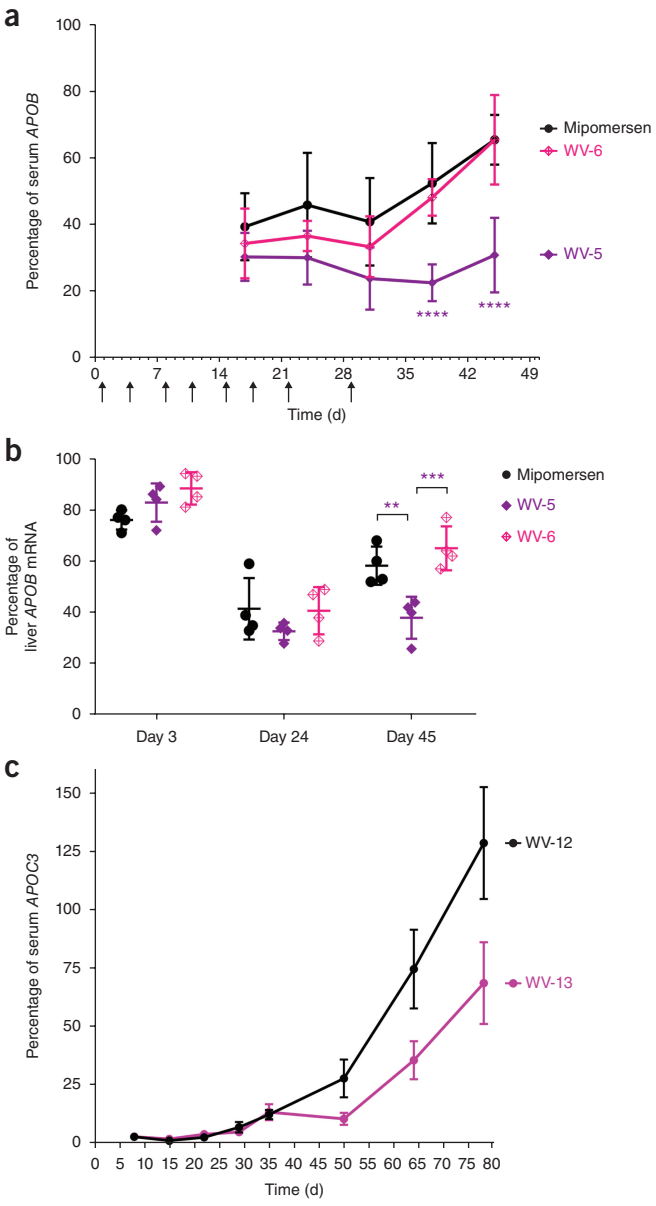

Figure 5 *In vivo* serum APOB and APOC3 protein kinetics in transgenic mice that were treated with mixtures or stereopure ASOs. (**a**) The stereopure WV-5 with an SSR core yields a more durable serum APOB response than mipomersen or other stereopure ASOs. Percentage of serum APOB compared with pre-bleed is plotted with respect to time. Arrows under *x* axis indicate doses of ASO (10 mg per kg; $n = 4$ for each time point). Error bars indicate s.d. $^{****}P \leq 0.0001$ in two-way ANOVA followed by Newman–Keuls *post hoc* test. (**b**) *In vivo* liver *APOB100* mRNA kinetics in the transgenic mice treated with mipomersen or stereopure components at days 3, 24 and 45 ($n = 4$ for each time point). Error bars indicate s.d. $^{**}P \leq 0.01$, $^{***}P \leq 0.001$ in two-way ANOVA. (**c**) The stereopure WV-13 with an SSR code in its core yields a more durable serum APOC3 response than the stereorandom mixture (WV-12). Percentage of serum APOC3 levels in ASO-treated mice compared with saline-treated mice with respect to time (5 mg per kg, $n = 5$ for each time point). Error bars indicate s.e.m.

serum APOB100 levels by day 17. The duration of the response, however, differed among the ASOs. By day 31, APOB100 levels in mice treated with mipomersen or WV-6 began to rise, whereas APOB100 levels in mice treated with WV-5 remained at low levels (~70% lower than baseline) until the mice were euthanized at day 45, with statistically significant differences at days 38 and 40 ($P \leq 0.0001$, $n = 4$ mice per group). The other ASOs were less potent than mipomersen but were comparably durable (**Supplementary Fig. 7**). *APOB100* mRNA levels in the liver dropped substantially for all ASOs by day 24, but began to recover by day 45 in response to WV-6 and mipomersen, whereas the response to WV-5 persisted ($P \leq 0.01$, $n = 4$ mice per group, two-way ANOVA). Differences in the duration of activity were not attributable to the persistence of mipomersen or its stereopure components, as the concentration of the ASOs did not differ substantially at any time assayed.

To demonstrate that the impact of PS stereochemistry is not limited to an ASO with the sequence or chemistry of mipomersen, we generated WV-13, which incorporates the SSR stereochemical code, targets human *APOC3* mRNA, and is chemically modified with GalNAc to improve delivery to the liver[28], and WV-12, a stereorandom control (**Supplementary Fig. 8**). Following three subcutaneous injections into human *APOC3* transgenic mice[29], we evaluated APOC3 serum protein levels for 11 weeks. Consistent with the APOB100 results, WV-13 and WV-12 comparably decreased APOC3 protein levels, but the stereopure ASO yielded a more durable response; as with the mipomersen study, these differences were not attributable to differences in the concentration of the ASOs in the liver, which were not substantially different even at day 78 (**Fig. 5c** and **Supplementary Fig. 9**). Taken together, these data indicate that stereopure ASOs containing the *SSR* stereochemical code improve the durability of *in vivo* response, independent of sequence, and this improved activity is not limited to gapmer ASOs.

DISCUSSION

We developed the SOSICS method to enable rapid, practical, and scalable synthesis of stereopure oligonucleotides bearing PS linkages, with the stereochemistry being programmable at each internucleotide linkage. The approach combines an oxazaphospholidine method[12] and the direct conversion of a phosphite having a tertiary alcohol into an *S*-alkyl phosphorothioate via an Arbusov-type mechanism. Using SOSICS, we synthesized stereopure PS ASOs composed of 2′-deoxyribonucleosides. In addition, we demonstrated that the method worked efficiently with oligonucleotides bearing the bulky 2′-MOE substituent, giving greater than 99% stereochemical selectivity with high coupling efficiency to furnish sufficient amounts of stereochemically pure ASOs for studies in animal models. The SOSICS method is readily adaptable for pharmaceutical-scale ASO production.

Using rationally designed stereopure versions of mipomersen, we discovered that PS stereochemistry affects every physicochemical and pharmacologic property that we examined; the behaviors of individual oligonucleotides were distinct from each other and from mipomersen; and *Sp* linkages increased the lipophilicity and stability of ASOs *in vitro*. Indeed, we show that *Sp* linkages in the ends of an ASO gapmer can replace the stabilizing activity of 2′-MOE-modified nucleotides. We also report a stereochemical code (*SSR*) in the DNA core of the PS ASO that is recognized by RNase H1 and enhanced activity *in vitro* and *in vivo*. Although others have reported modest differences in the RNase H1 activity of gapmer ASOs with all-*Rp* or all-*Sp* cores compared with a stereorandom mixture[30], they concluded that PS-linkage stereochemistry in the DNA core provides no benefits for therapeutic application relative to the stereorandom mixture. That study, however, failed to determine or examine the stereochemical configuration that affords optimal RNase H1 activity. By contrast, our data demonstrate that optimal position-specific stereochemistry (*SSR*) increased activity of WV-5 compared with mipomersen both *in vitro* and *in vivo*. This *SSR* code may minimize the need for medicinal chemists to screen a daunting number of stereoisomers to identify active ASOs.

Because APOB100 expression levels in mice in the wash-out period were substantially lower for WV-5 than for mipomersen, it is possible that lower or less frequent doses of WV-5 could yield therapeutic efficacy equivalent to mipomersen. Indeed, several *P*-stereochemically pure diastereomers that are components of mipomersen were either less potent *in vivo* than the mixture or not active at all. This finding indicates that components of mipomersen that contribute to the drug load in the patient (limiting the dose and potentially contributing toxicity) are not meaningfully active. We also demonstrate that this *SSR* code improved the durability of *in vivo* response independent of sequence, as a stereopure ASO targeting human *APOC3* also yielded a more durable response than its stereorandom counterpart. This ASO also included chemical modifications (GalNAc) that would already be expected to improve its activity compared with a standard gapmer.

Optimization of ASOs for efficient cleavage of the target mRNA by RNase H1 is critical. It is notable that prior studies using stereochemically pure diastereomers have suggested *Rp* PS DNAs are the best substrate for RNase H1 (refs. 24,25,31). Since the nuclease stability of *Rp* PS DNAs is not favorable, the industry settled on mixtures, assuming that some components impart stability and others impart activity[30,32]. Our work provides evidence that stability and activity can be rationally engineered into the same molecule. These findings demonstrate that PS stereochemistry affects the measurable biophysical and biochemical properties of ASOs, and in certain cases, for example, with regards to nucleolytic stability, the observed impact is substantial. It is reasonable, therefore, to expect that precise control over the stereochemistry of ASOs will enable the development of drugs with improved clinical efficacy, and perhaps safety, compared with those comprising complex mixtures, each component of which exhibits its own pharmacologic properties.

We believe the SOSICS method provides a versatile approach for the production of stereopure backbone-modified oligonucleotides applicable in the synthesis of stereopure PS–PO chimeric oligonucleotides, *P*-stereochemically pure siRNA[33,34] and splice-switching oligonucleotide therapeutics[35].

METHODS

Methods, including statements of data availability and any associated accession codes and references, are available in the online version of the paper.

Note: Any Supplementary Information and Source Data files are available in the online version of the paper.

ACKNOWLEDGMENTS

We thank S. Mathieu, D. Boulay, S. Divakaramenon, K. Bowman, V. Vathipadiekal, M. Melkonian, J.C. Dodart, H. Yang, Y. (Benny) Yin, F. Desai and Z. Zhong of Wave Life Sciences for helpful discussions and support for experiments. We thank T. Wada of Tokyo University of Science for general discussions regarding the original oxazaphospholidine method. We thank U. Shigdel of Harvard University (present affiliation, Warp Drive Bio) for purifying the human RNase HC protein. We thank W. Yang of National Institute of Diabetes and Digestive and Kidney Diseases for providing the human RNase HC clone. While at RA Capital Management, A. Donner (present affiliation, The Chemical Probes Portal) provided expert assistance on production of the manuscript.

AUTHOR CONTRIBUTIONS

All authors contributed to the designing, planning and/or data collection of this project. N.I. designed and developed the SOSICS platform. N.I., D.C.D.B., I.Z., S.M.S. and G.L. carried out the synthesis and characterization of ASOs and reagents. N.I. and Meena conducted rat liver homogenate stability studies and rat serum stability studies. N.I., S.M., N.S. and Meena conducted RNase HC cleavage studies. N.S., L.H.A., M.F.-K. and J.J.Z. performed *in vitro* and *in vivo* biological analyses. N.I. and G.L.V. wrote the manuscript, and all authors refined the manuscript.

COMPETING FINANCIAL INTERESTS

The authors declare competing financial interests: details are available in the online version of the paper.

1. Crooke, S.T. Molecular mechanisms of action of antisense drugs. *Biochim. Biophys. Acta* **1489**, 31–44 (1999).
2. Deleavey, G.F. & Damha, M.J. Designing chemically modified oligonucleotides for targeted gene silencing. *Chem. Biol.* **19**, 937–954 (2012).
3. Swayze, E.E. *et al.* Antisense oligonucleotides containing locked nucleic acid improve potency but cause significant hepatotoxicity in animals. *Nucleic Acids Res.* **35**, 687–700 (2007).
4. Sharma, V.K., Sharma, R.K. & Singh, S.K. Antisense oligonucleotides: modifications and clinical trials. *MedChemComm.* **5**, 1454–1471 (2014).
5. Eckstein, F. Phosphorothioates, essential components of therapeutic oligonucleotides. *Nucleic Acid Ther.* **24**, 374–387 (2014).
6. Crooke, S.T. & Geary, R.S. Clinical pharmacological properties of mipomersen (Kynamro), a second generation antisense inhibitor of apolipoprotein B. *Br. J. Clin. Pharmacol.* **76**, 269–276 (2013).
7. Stec, W.J., Grajkowski, A., Koziolkiewicz, M. & Uznanski, B. Novel route to oligo (deoxyribonucleoside phosphorothioates). Stereocontrolled synthesis of P-chiral oligo(deoxyribonucleoside phosphorothioates). *Nucleic Acids Res.* **19**, 5883–5888 (1991).
8. Stec, W.J. *et al.* Deoxyribonucleoside 3′-O-(2-thio- and 2-oxo-"spiro"-4, 4-pentamethylene-1,3,2-oxathiaphospholane)s: monomers for stereocontrolled synthesis of oligo(deoxyribonucleoside phosphorothioate)s and chimeric PS/PO Oligonucleotides. *J. Am. Chem. Soc.* **120**, 7156–7167 (1998).
9. Iyer, R.P., Yu, D., Ho, N.-H., Tan, W. & Agrawal, S. A novel nucleotide phosphoramidite synthon derived from1R, 2S-ephedrine. *Tetrahedron Asymmetry* **6**, 1051–1054 (1995).
10. Guo, M., Yu, D., Iyer, R.P. & Agrawal, S. Solid-phase stereoselective synthesis of 2′-O-methyl-oligoribonucleoside phosphorothioates using nucleoside bicyclic oxazaphospholidines. *Bioorg. Med. Chem. Lett.* **8**, 2539–2544 (1998).
11. Wilk, A., Grajkowski, A., Phillips, L.R. & Beaucage, S.L. Deoxyribonucleoside cyclic N-acylphosphoramidites as a new class of monomers for the stereocontrolled synthesis of oligothymidylyl- and oligodeoxycytidylyl- phosphorothioates. *J. Am. Chem. Soc.* **122**, 2149–2156 (2000).
12. Oka, N., Yamamoto, M., Sato, T. & Wada, T. Solid-phase synthesis of stereoregular oligodeoxyribonucleoside phosphorothioates using bicyclic oxazaphospholidine derivatives as monomer units. *J. Am. Chem. Soc.* **130**, 16031–16037 (2008).
13. Nukaga, Y., Yamada, K., Ogata, T., Oka, N. & Wada, T. Stereocontrolled solid-phase synthesis of phosphorothioate oligoribonucleotides using 2′-O-(2-cyanoethoxymethyl)-nucleoside 3′-O-oxazaphospholidine monomers. *J. Org. Chem.* **77**, 7913–7922 (2012).
14. Oka, N., Kondo, T., Fujiwara, S., Maizuru, Y. & Wada, T. Stereocontrolled synthesis of oligoribonucleoside phosphorothioates by an oxazaphospholidine approach. *Org. Lett.* **11**, 967–970 (2009).
15. Li, M. *et al.* Synthesis and cellular activity of stereochemically-pure 2′-O-(2-methoxyethyl)-phosphorothioate oligonucleotides. *Chem. Commun. (Camb.)* **53**, 541–544 (2017).
16. Iwamoto, N., Oka, N., Sato, T. & Wada, T. Stereocontrolled solid-phase synthesis of oligonucleoside H-phosphonates by an oxazaphospholidine approach. *Angew. Chem. Int. Edn Engl.* **48**, 496–499 (2009).
17. Brill, W.K.-D. Thioalkylation of nucleoside-H-phosphonates and its application to solid phase synthesis of oligonucleotides. *Tetrahedr. Lett.* **36**, 703–706 (1995).
18. Nielsen, J. & Caruthers, M.H. Directed Arbuzov-type reactions of 2-cyano-1, 1-dimethylethyl deoxynucleoside phosphites. *J. Am. Chem. Soc.* **110**, 6275–6276 (1988).
19. Nowotny, M. *et al.* Structure of human RNase H1 complexed with an RNA/DNA hybrid: insight into HIV reverse transcription. *Mol. Cell* **28**, 264–276 (2007).
20. Boczkowska, M., Guga, P. & Stec, W.J. Stereodefined phosphorothioate analogues of DNA: relative thermodynamic stability of the model PS-DNA/DNA and PS-DNA/RNA complexes. *Biochemistry* **41**, 12483–12487 (2002).
21. Oka, N. & Wada, T. Stereocontrolled synthesis of oligonucleotide analogs containing chiral internucleotidic phosphorus atoms. *Chem. Soc. Rev.* **40**, 5829–5843 (2011).
22. Koziołkiewicz, M. *et al.* Stability of stereoregular oligo(nucleoside phosphorothioate)s in human plasma: diastereoselectivity of plasma 3′-exonuclease. *Antisense Nucleic Acid Drug Dev.* **7**, 43–48 (1997).
23. Lima, W.F. *et al.* Human RNase H1 discriminates between subtle variations in the structure of the heteroduplex substrate. *Mol. Pharmacol.* **71**, 83–91 (2007).
24. Koziolkiewicz, M., Krakowiak, A., Kwinkowski, M., Boczkowska, M. & Stec, W.J. Stereodifferentiation--the effect of P chirality of oligo(nucleoside phosphorothioates) on the activity of bacterial RNase H. *Nucleic Acids Res.* **23**, 5000–5005 (1995).
25. Yu, D. *et al.* Stereo-enriched phosphorothioate oligodeoxynucleotides: synthesis, biophysical and biological properties. *Bioorg. Med. Chem.* **8**, 275–284 (2000).
26. Watts, J.K. & Corey, D.R. Silencing disease genes in the laboratory and the clinic. *J. Pathol.* **226**, 365–379 (2012).
27. Linton, M.F. *et al.* Transgenic mice expressing high plasma concentrations of human apolipoprotein B100 and lipoprotein(a). *J. Clin. Invest.* **92**, 3029–3037 (1993).
28. Prakash, T.P. *et al.* Targeted delivery of antisense oligonucleotides to hepatocytes using triantennary N-acetyl galactosamine improves potency 10-fold in mice. *Nucleic Acids Res.* **42**, 8796–8807 (2014).
29. Reaven, G.M., Mondon, C.E., Chen, Y.D. & Breslow, J.L. Hypertriglyceridemic mice transgenic for the human apolipoprotein C-III gene are neither insulin resistant nor hyperinsulinemic. *J. Lipid Res.* **35**, 820–824 (1994).
30. Wan, W.B. *et al.* Synthesis, biophysical properties and biological activity of second generation antisense oligonucleotides containing chiral phosphorothioate linkages. *Nucleic Acids Res.* **42**, 13456–13468 (2014).
31. Stec, W.J. *et al.* Stereodependent inhibition of plasminogen activator inhibitor type 1 by phosphorothioate oligonucleotides: proof of sequence specificity in cell culture and in vivo rat experiments. *Antisense Nucleic Acid Drug Dev.* **7**, 567–573 (1997).
32. Krieg, A.M., Guga, P. & Stec, W. P-chirality-dependent immune activation by phosphorothioate CpG oligodeoxynucleotides. *Oligonucleotides* **13**, 491–499 (2003).
33. Bumcrot, D., Manoharan, M., Koteliansky, V. & Sah, D.W. RNAi therapeutics: a potential new class of pharmaceutical drugs. *Nat. Chem. Biol.* **2**, 711–719 (2006).
34. Jahns, H. *et al.* Stereochemical bias introduced during RNA synthesis modulates the activity of phosphorothioate siRNAs. *Nat. Commun.* **6**, 6317 (2015).
35. Hammond, S.M. & Wood, M.J. Genetic therapies for RNA mis-splicing diseases. *Trends Genet.* **27**, 196–205 (2011).

ONLINE METHODS

Materials. Dry organic solvents were purchased and prepared by appropriate procedures before use. The other organic solvents were reagent grade and used as received. NMR spectra (^{1}H NMR, ^{13}C NMR and ^{31}P NMR) were recorded with the appropriate reference on a Varian MERCURY 300, 400 or 500 NMR spectrometer or Brukar BioSpin GmbH NMR spectrometer. ESI high-resolution mass spectra were recorded on an Agilent 6230 ESI TOF (see also **Life Sciences Reporting Summary**).

Synthesis and purification of *P*-stereocontrolled PS-oligonucleotides is detailed in **Supplementary Methods**.

Thermal denaturation (Tm). Equimolar amounts of RNA and each ASO were dissolved in 1× PBS to obtain a final concentration of 1 μM of each strand. Duplex samples were then annealed by heating at 90 °C, followed by slow cooling to 4 °C and storage at 4 °C. UV absorbance at 254 nm was recorded at intervals of 30 s as the temperature was raised from 15 °C to 95 °C at a rate of +0.5 °C per min, using a Cary Series UV-Vis spectrophotometer (Agilent Technologies). Absorbance was plotted against the temperature and the Tm values were calculated by taking the first derivative of each curve.

Human RNase HC expression and purification. Human RNase HC clone was obtained from Wei Yang's laboratory (NIH, Bethesda, MD). The published protocol was followed for expressing and purifying human RNase HC (residues 136-286)[19] with the following exceptions: an SP column was used after desalt and buffer exchange and the His-tag was not removed.

Determination of initial velocities. Duplexes were prepared as previously described for the *in vitro* RNase HC activity assay ($n = 3$). For determination of the initial velocities, each RNase HC reaction contained 20 μM ASO–RNA duplex in 1× RNase H buffer (75 mM KCl, 50 mM Tris-HCl, 3 mM $MgCl_2$, 10 mM dithiothreitol, pH = 8.3) in a reaction volume of 67.5 μL. The mixture was pre-incubated at 37 °C for 10 min before addition of 7.5 μL of RNase HC enzyme (0.4 μM) with final concentrations of 20.0 μM substrate and 0.04 μM RNase HC (500:1 ratio). A 7 μL aliquot of the cleavage reaction was removed and quenched at time points ranging from 20 s to 120 s into 30 μL of 50 mM solution of EDTA. The reaction mixture quenched at each time point was analyzed by the method described above for *in vitro* RNase HC activity to determine the amount of RNA cleaved. The concentration of the converted product was then plotted as a function of time. The initial cleavage rate was obtained from the slope (nmole of total RNA cleavage products per min) of the best fit line for the initial linear portion of the reaction rate curve.

Cellular potency assay. Lipofectamine 2000-formulated ASOs were transfected into Hep3B cells (https://www.atcc.org/Products/All/HB-8064.aspx) using a standard reverse transfection protocol. Eight concentrations for each ASO were tested (1:4 dilutions) with 50 nM as the highest concentration. Cells were harvested 24-h post transfection. Post-transfection *APOB100* mRNA levels were evaluated via real-time PCR and the values normalized to GAPDH as an endogenous control. IC_{50}s were calculated by fitting the 4-parameter logistic regression model in Graphpad Prism 6.01. We performed the experiment in triplicate ($n = 3$).

Animals. VivoPath (Worcester, MA) carried out the in-life portion of all rodent experiments in a blinded fashion. All experiments were conducted under a protocol approved by VivoPath's Animal Care and Use Committee.

For whole rat liver homogenates, male Sprague-Dawley rats (Charles River Laboratories) were anesthetized with an intraperitoneal (IP) injection of sodium pentobarbital solution, before infusion of 500 mL of cold saline via the hepatic portal vein to perfuse the liver. Livers were then harvested and maintained on ice until minced. Five mL of cold homogenization buffer (100 mM Tris pH 8.0, 1 mM magnesium acetate, with antibiotic and antimycotic agents) was added per gram of liver tissue, and then homogenization was carried out with a QIAGEN TissueRuptor tissue homogenizer while maintaining the tube on ice. Protein concentrations were determined using a BCA protein assay (Pierce). Liver homogenates were stored at −60 °C.

In vivo studies. C57BL/6NTac-TgN(APOB100) transgenic mice (Female, Taconic (Germantown, NY)), which express human Apolipoprotein B-100, were genotyped before delivery. Mice were allowed to acclimate to the facility for at least 7 d before study start. All mice had access to regular chow and water *ad libitum*.

Mipomersen dose-finding study. To determine the most appropriate dose of mipomersen and its components for *in vivo* studies, a dose-titration analysis for mipomersen was performed. Mice randomized to dosage groups (15–19 weeks old, $n = 5$ per group) were dosed in a blinded manner with 0 (PBS), 2.5, 5, 10 or 25 mg/kg mipomersen via IP injection. Blood was collected by submandibular (cheek) bleed (days 17 and 24), and mice were euthanized by cardiac puncture (day 24); blood was then processed to serum. APOB100 levels in the serum were normalized to the PBS control cohort. A dose of 10 mg/kg, resulting in low to intermediate suppression of serum APOB100 levels, was chosen for evaluation of mipomersen components.

Comparative studies. Mipomersen, WV-5 and WV-6 were used to dose, in a blinded manner, randomized mice by IP injection (12 weeks old, $n = 4$) at 10 mg/kg on days 1, 4, 8, 11, 15, 18, 22 and 29. Blood was collected on days 0 (the day before first dose, used as analysis normalization control), 17, 24, 31 and 38 by cheek bleed and at euthanization on day 45 by cardiac puncture; blood was then processed to serum. Randomized mice were dosed by mipomersen, WV-1, WV-2, WV-3 and WV-4 to by IP injection (15–19 weeks old, $n = 5$) at 10 mg/kg on days 1, 4, 8, 11, 15, 18, 22, 25, 29 and 32. Blood was collected on days 0, 17, 24, 31, 38, 45, 52 and 60 by cheek bleed, and mice were euthanized on day 66 by cardiac puncture; blood was then processed to serum. In this experiment, serum levels of APOB100 were normalized to those from PBS-injected control mice ($n = 5$). Thus, these two studies are not directly comparable in terms of magnitude of response (y axis) but are comparable for duration of response.

Human APOC3 transgenic mice B6;CBA-Tg(APOC3)3707Bres/J were obtained from The Jackson Laboratory and animal experiments were performed in accordance with approved guidelines and ethical approval from Biomere Institutional Animal Care and Use Committee. Adult male mice 3 months of age were housed in cages on a 12 h light-dark cycle with controlled temperature and humidity and were given access to food and water *ad libitum*. Three doses, delivered every other day beginning on day 1, of 1× PBS or ASO at 5 mg per kg were injected subcutaneously in a blinded manner. We collected blood by tail vein nick under anesthesia. After collection, whole blood was allowed to clot at room temperature for 30 min, and serum was separated by centrifugation at 2,000*g* for 10 min under refrigeration.

Protein quantification. APOB protein in serum was measured using an ELISA kit specific for human Apolipoprotein B (Abcam: ab108807). Data were normalized to PBS-treated control animals or day 0, pre-bleed samples (see Animals). Serum samples were diluted to fall within the linear range of the standard curve, and assayed per the kit recommended protocol without modification. Automated washes were done with 30 s soaks using an Aquamax 4000 (Molecular Devices). Reactions were stopped after 8–10 min incubation with Chromogen substrate, and measurements were taken with a Spectramax M5 (Molecular Devices). Standard curves were generated by plotting the standard concentration on the x axis and the corresponding mean 450 nm absorbance on the y axis. The best-fit line was determined by regression analysis using log-log curve-fit. A high criterion of $R^2 > 0.98$ was set for absolute quantification. Each assay plate included a negative (pre-bleed) and a positive (mipomersen-treated) control, and each serum sample was assayed in three technical replicates. For technical replicates, the mean absolute level of APOB was normalized to the mean value of a PBS-treated sample or its respective pre-bleed sample group to obtain the relative level of APOB protein expression. Relative levels of APOB protein expression were used for statistical analyses (Graphpad Prism) by 2-way ANOVA.

For APOC3 serum protein analysis, 3 μL of serum was serially diluted to 1:100,000 and analyzed by commercially available ELISA assays (Abcam, Cat# ab154131) as recommended by the vendor. Samples from ASO-treated animals were compared with those from saline-treated animals. Highly hemolyzed serum samples were excluded from analysis by visual assessment[38]. Relative levels of APOC3 protein expression were used for statistical analyses (Graphpad Prism) by two-way ANOVA.

***APOB100* mRNA quantification.** The livers of treated mice were flash frozen upon collection and stored at −80 °C before grinding into a fine powder.

doi:10.1038/nbt.3948

Approximately 25 mg of powdered mouse liver was used for total RNA extraction with a high-throughput Qiazol based kit 96 RNeasy 96 Universal Tissue Kit (Qiagen). A High-Capacity cDNA kit (Life Technologies: #4374967) was used for complementary DNA synthesis on a Bio-Rad C1000 thermal cycler. *APOB* mRNA levels were measured using quantitative PCR using the primers (forward: 5′-TGCTAAAGGCACATATGGCCT-3′, reverse: 5′-CTCAGGTTGGACTCTCCATTGAG-3′) and probe (5′-6-FAM-CTTGTCAG AGGGATCCTAACACTGGCCG-TAMRA). VIC-labeled GAPDH master mix was used to measure *GAPDH* as the housekeeping control (Life Technologies: 4352339E Mouse GAPD (GAPDH) Endogenous Control Primer Limited). An untreated baseline was established by averaging human *APOB* mRNA levels for an untreated group. All samples were processed together and were analyzed on the same plate. Statistical analysis of human *APOB* mRNA expression was performed with Graphpad Prism by 2-way ANOVA.

Quantification of ASOs in liver. LC/MS method for ASOs for APOB100:25 mg of powered liver tissue was weighed in Thermo tubes, which were kept on dry ice for at least 5 min. While the tubes were still in dry ice, caps were removed and Proteinase K (6 µL of 20 mg/mL) and 200 µL 1× Buffer (0.5% IGEPAL, 0.1 M NaCl, 5 mM EDTA, 10 mM Tris-HCl, pH = 8.0) were added, and the tubes were vortexed and removed from dry ice. A 27-mer ASO control (5′- GCGTTTGCTCTTCTTCTTGCGTTTTTT-3′, where underlined bases are 2-MOE modified, all internucleotidic linkages are modified with PS and C is 5MeC in all instances) (2.5 µL of 100 µg/mL) was added to each tube. The samples were heated at 60 °C for 30 min while shaking at 900 r.p.m. and cooled on ice. 50 µL ammonium hydroxide was added to each tube followed by 200 µL chloroform:phenol:isoamyl alcohol (25:24:1, v/v/v). All samples were vortexed for 30 s and then centrifuged at 7,000 r.p.m. The aqueous layer (340 µL) was separated and dried in Speedvac. The residue was reconstituted in 100 µL water; 20 µL was analyzed by liquid-chromatography-coupled triple quadrupole mass spectrometry (ABSCIEX QTRAP 5500 LC-MS/MS) after 20× dilution in water. Samples were injected onto a Chromolith Performance RP-18e column (3.1 × 100 mm) using a PE 200 Series Micro Pump LC system at a flow rate of 1.6 mL/min using the mobile phase A (2 mM TEA, 40 mM HFIP) and mobile phase B (100% Methanol). A 1.8-min gradient was utilized going from 5% to 85% (1.0 min) to 95% (2.3 min) of Mobile Phase B for a total run time of 3.0 min. The mass spectrometer was operated at unit resolution for Q1 and Q3 quadrupoles. We detected the oligonucleotides using selected reaction monitoring mode for the following transitions involving loss of phosphate from intact oligonucleotide: m/z 896.5 → 94.9 for Mipomersen, WV-5 and WV-6; m/z 855.9 → 94.9 for 27-mer internal standard. MS analysis was carried out at Charles River Laboratories (Wilmington, MA). Calibration curves for mipomersen, WV-5, and WV-6 were generated via the same protocol with a concentration range of 5–500 µg/mL.

Hybridization ELISA for APOC3 ASOs. One part of liver tissue (Day 78) was disrupted in four parts of lysis buffer (0.5% IGEPAL, 100 mM NaCl, 5 mM EDTA, 10 mM Tris·HCl pH 8, 600 µg/mL proteinase K) by Precellys Evolution (Bertin Technologies), incubated at 60 °C for 30 min, aliquoted into a 96-well plate for −80 °C storage and serving as source plate. A maleic-anhydride-activated 96-well plate (Pierce 15110) was coated with 50 µL of capture probe (5AmMC12 (5′-amino modifier C12)- ATAAAGCTGG, where underlined bases are locked nucleic acid (LNA) modified (Exigon)) at 500 nM in 2.5% $NaHCO_3$ (Gibco, 25080-094) for 2 h at 37 °C. The plate was then washed three times with PBST (PBS + 0.1% Tween-20), blocked with 5% fat free milk-PBST at 37 °C for 1 h. Payload ASO was serial-diluted into matrix (naive tissue lysates) starting at 50 ng/mL. This standard, together with original samples, were diluted with lysis buffer (4 M guanidine; 0.33% *N*-lauryl sarcosine; 25 mM sodium citrate; 10 mM DTT) so that the amount of ASO in all samples was less than 50 ng/ml. 20 µL of diluted samples were mixed with 180 µL of 333 nM detection probe (ACAAGAAGCT-3BioTEG (3′-Biotin TEG), where underlined bases are LNA-modified (Exigon)), diluted in PBST, then denatured in a PCR machine (65 °C, 10 min, 95 °C, 15 min, 4 °C ∞). 50 µL of denatured samples was distributed in blocked ELISA plate in duplicates, and incubated overnight at 4 °C. After three washes of PBST, 1:2,000 streptavidin-AP in PBST was added, 50 µL per well and incubated at room temperature for 1 h. After an extensive wash with PBST, 100 µL of AttoPhos (Promega S1000) was added, incubated at room temperature in dark for 10 min and read on a plate reader (Molecular Device, M5) fluorescence channel: Ex435nm, Em555nm. The ASO in samples were calculated according to standard curve by four-parameter curve fit.

Statistics. For *in vitro* biochemical experiments (stability in rat liver homogenate, stability in rat serum, RNase HC activity and V_0 calculations), data were collected as triplicate of individual experiments for each time point ($n = 3$). Data were assessed by two-way ANOVA. For cellular IC_{50} calculations, data were collected as triplicates of individual experiments for each time point ($n = 3$). Curves were calculated using a four-parameter logistic regression model in GraphPad Prism 6.01, and were assessed by 2-way ANOVA. In APOB *in vivo* experiments, serum samples were assessed in triplicate technical replicates ($n = 3$) for each independent experiment ($n = 4$ mice per time point per treatment). Liver mRNA and ASO quantification were performed for the individual experiments ($n = 4$ per time point per treatment). For APOC *in vivo* experiments, serum samples from individual experiments were processed ($n = 5$). Liver ASO quantification was also performed for each individual experiments ($n = 5$). All *in vivo* data were assessed by 2-way ANOVA.

Data availability statement. Authors confirm that all relevant data are included in the paper and/or its supplementary information files.

36. Østergaard, M.E. *et al.* Efficient synthesis and biological evaluation of 5′-GalNAc conjugated antisense oligonucleotides. *Bioconjug. Chem.* **26**, 1451–1455 (2015).
37. Aaronson, J.G. *et al.* Rapid HATU-mediated solution phase siRNA conjugation. *Bioconjug. Chem.* **22**, 1723–1728 (2011).
38. Koseoglu, M., Hur, A., Atay, A. & Cuhadar, S. Effects of hemolysis interferences on routine biochemistry parameters. *Biochem. Med. (Zagreb)* **21**, 79–85 (2011).

Corresponding Author: Gregory L. Verdine

Date: Jul 24, 2017

Life Sciences Reporting Summary

Nature Research wishes to improve the reproducibility of the work we publish. This form is published with all life science papers and is intended to promote consistency and transparency in reporting. All life sciences submissions use this form; while some list items might not apply to an individual manuscript, all fields must be completed for clarity.

For further information on the points included in this form, see Reporting Life Sciences Research. For further information on Nature Research policies, including our data availability policy, see Authors & Referees and the Editorial Policy Checklist.

Experimental design

1. Sample size

   Describe how sample size was determined.

   No effect size was predetermined. All the biochemical and biological experiments were performed in three replicated or more.

2. Data exclusions

   Describe any data exclusions.

   Highly hemolized serum samples were excluded from analysis by visual assessment. Reported in Online methods: page 55, Koseoglu et al. 2011

3. Replication

   Describe whether the experimental findings were reliably reproduced.

   All attempts at replication were successful.

4. Randomization

   Describe how samples/organisms/participants were allocated into experimental groups.

   The dosing groups were filled by randomly selecting from the same pool of animals for in vivo experiments.

5. Blinding

   Describe whether the investigators were blinded to group allocation during data collection and/or analysis.

   The investigator was blinded for in vivo experiments of all animal experiments.

   Note: all studies involving animals and/or human research participants must disclose whether blinding and randomization were used.

6. Statistical parameters

   For all figures and tables that use statistical methods, confirm that the following items are present in relevant figure legends (or the Methods section if additional space is needed).

n/a	Confirmed	
☐	☒	The exact sample size (*n*) for each experimental group/condition, given as a discrete number and unit of measurement (animals, litters, cultures, etc.)
☐	☒	A description of how samples were collected, noting whether measurements were taken from distinct samples or whether the same sample was measured repeatedly.
☐	☒	A statement indicating how many times each experiment was replicated
☐	☒	The statistical test(s) used and whether they are one- or two-sided (note: only common tests should be described solely by name; more complex techniques should be described in the Methods section)
☐	☒	A description of any assumptions or corrections, such as an adjustment for multiple comparisons
☐	☒	The test results (e.g. *p* values) given as exact values whenever possible and with confidence intervals noted
☐	☒	A summary of the descriptive statistics, including central tendency (e.g. median, mean) and variation (e.g. standard deviation, interquartile range)
☐	☒	Clearly defined error bars

See the web collection on statistics for biologists for further resources and guidance.

Nature Biotechnology: doi:10.1038/nbt.3948

Software

Policy information about availability of computer code

7. Software

Describe the software used to analyze the data in this study.	GraphPad Prism 6 or 7

For all studies, we encourage code deposition in a community repository (e.g. GitHub). Authors must make computer code available to editors and reviewers upon request. The *Nature Methods* guidance for providing algorithms and software for publication may be useful for any submission.

Materials and reagents

Policy information about availability of materials

8. Materials availability

Indicate whether there are restrictions on availability of unique materials or if these materials are only available for distribution by a for-profit company.	All unique materials used are readily available from the authors.

9. Antibodies

Describe the antibodies used and how they were validated for use in the system under study (i.e. assay and species).	Reported in Online Method: page 55.

10. Eukaryotic cell lines

a. State the source of each eukaryotic cell line used.	Reported in Online Method: page 52-53.
b. Describe the method of cell line authentication used.	Probe validatation demonstrated optimal expression of Apolipoprotein B. Cell morphology was cross-referenced and confirmed by microscopy.
c. Report whether the cell lines were tested for mycoplasma contamination.	The cell lines were not tested for mycoplasma contamination.
d. If any of the cell lines used in the paper are listed in the database of commonly misidentified cell lines maintained by ICLAC, provide a scientific rationale for their use.	No commonly identified cell lines were used.

Animals and human research participants

Policy information about studies involving animals; when reporting animal research, follow the ARRIVE guidelines

11. Description of research animals

Provide details on animals and/or animal-derived materials used in the study.	Reported in Online Method: page 53-55, 58.

Policy information about studies involving human research participants

12. Description of human research participants

Describe the covariate-relevant population characteristics of the human research participants.	The study did not involve human research participants.

Nature Biotechnology: doi:10.1038/nbt.3948